Efficient Measurement of the Orbital-Angular-Momentum Spectrum of an Electron Beam via a Dammann Vortex Grating

Yuuki Noguchi,[1] Shota Nakayama,[1] Takafumi Ishida,[2] Koh Saitoh,[2,*] and Masaya Uchida[3]

[1]*Department of Crystalline Materials Science, Nagoya University, Furo-cho, Chikusa-ku, Nagoya 464-8603, Japan*

[2]*Institute of Materials and Systems for Sustainability, Nagoya University, Furo-cho, Chikusa-ku, Nagoya 464-8603, Japan*

[3]*Advanced Science Research Laboratory, Saitama Institute of Technology, Fukaya, Saitama 369-0293, Japan*

Measuring the orbital-angular-momentum (OAM) states of electron beams is of great importance in diverse applications. Here, we demonstrate a method to effectively measure the OAM spectrum of an electron beam by exploiting a two-dimensional Dammann vortex grating (DVG). This grating enables us to simultaneously measure an input electron beam in a transmission electron microscope using its OAM components with values between $-10\hbar$ and $10\hbar$ (OAM spectrum). We then experimentally evaluate the performance of the DVG OAM analyzer when measuring electron beams generated by spiral zone plates and nanofabricated magnetic needles. Our evaluation supports the validity of this approach, which paves the way toward enabling a wide range of electron OAM applications, including in nanoscale imaging and in materials science.

I. INTRODUCTION

The orbital angular momentum (OAM) of free electrons is a new degree of freedom that has attracted considerable attention in the past decade in fundamental research and for potential applications and is now an established area of research [1–9]. For instance, OAM allows us to probe the nanoscale magnetism of materials [10,11]. An electron beam with a spiraling phase structure $\exp(im\varphi)$ carries a well-defined quantized OAM value of $m\hbar$ per electron, where m is an integer, $\hbar$ is the reduced Planck constant, and φ is the azimuthal angle in the plane transverse to the beam axis. Such a characteristic phase structure yields ring-shaped intensity profiles. A variety of methods for generating electron beams carrying OAM have been reported, including by a phase plate [1], amplitude and phase forked gratings [2,3,12], spiral zone plates (SZPs) [13,14], nanoscale magnetic needles [15,16], polygonal slits [17], electrostatic generation [18,19], and so on. Electron OAM can be transferred via various scattering processes between an incident beam and a scatterer, such as an atom and a solid. As is the case for generation methods, the techniques and devices used to measure the OAM of electrons are of great significance to novel scattering and spectroscopy experiments [11,20–25].

In general, the OAM of electrons can be detected by observing the interference patterns [1,21,22]. However, it is not easy to simultaneously measure the OAM content of an input electron beam consisting of various OAM states. For example, it would be necessary to use noninterferometric methods in order to measure OAM for inelastic scattering experiments with electron beams involving OAM. Recently, a nondestructive method using induced currents has been proposed to measure electron OAM [24]. Very recently, Grillo *et al.* have demonstrated the performance of a device based on nanoscale holograms, which is realized by means of a log-polar coordinate transformation for measuring electron OAM components [11]. In their study, two delicate nanofabricated phase plates were implemented. Previously, based on the principle of reciprocity, we measured electron OAM by using a nanofabricated forked grating in a transmission electron microscope (TEM) [20]. Our experimental results indicated that it was possible to count electrons in response to their individual OAM values. Though this method was quite simple, the forked grating hindered us from obtaining high-order diffractions. In order to solve this problem of obtaining the entire OAM spectrum, here we propose a method for effectively measuring electron OAM via a two-dimensional (2D) Dammann vortex grating (DVG), which can generate an equal-intensity array among all of the desired diffraction orders. By using this device analyzer, we demonstrated the extraction of superposed OAM components of electrons with OAM values between $-10\hbar$ and $10\hbar$.

---

*saitoh@imass.nagoya-u.ac.jp

II. GRATING DESIGN AND METHODS

The DVGs we used here measure electron OAM in the same way as the forked grating we proposed previously [20]. The forked grating with a topological charge b transfers the OAM of $nb\hbar$ to the nth diffracted beam. A vortex beam with nonzero OAM has a ring-shaped intensity with zero intensity at the beam center, whereas a beam with zero OAM has nonzero intensity at the beam center. Therefore, the OAM of an input beam could be obtained by measuring the intensity at the beam center of the diffracted beam after it passes through the forked grating. We used DVGs in place of the forked grating. Dammann gratings, which have been used in the field of optics, are binary-phase optical gratings capable of generating one-dimensional (1D) or 2D equal-intensity beam arrays with high uniformity [26–28]. By combining Dammann gratings with forked gratings (i.e., DVGs), equal-intensity OAM beams among all of the desired diffraction orders can be obtained [29,30]. The application of DVGs to electrons has not been reported previously. Such DVGs enable us to measure the OAM content of input electrons for the desired OAM values in a single round.

Conventional Dammann gratings are binary-phase gratings with phase values of 0 and π. Although phase gratings for electrons are possible, they easily suffer from problems of charging and contamination in electron beams. Therefore, we elected to make binary-amplitude DVGs (see the Supplemental Material [31]). Although the diffraction efficiency of the amplitude grating is lower than that of the phase grating, and the relative intensity of the transmitted beam is enhanced more than that for a phase grating with a $(0, \pi)$ binary-phase structure, an amplitude grating is simple to make. An additional advantage of an amplitude grating is its smaller dependence on the wavelength of input electrons. Figure 1(a) shows a designed 2D DVG pattern that generates a 2×2 diffraction beam array, integrating the grating pattern with $m = 1$ and $m = 4$.

A binary-amplitude 2D DVG is fabricated using a focused-ion beam (FIB) instrument (Hitachi FB-2100) from a 2-μm-thick platinum/palladium (PtPd) film deposited on both sides of a thin (50 nm) silicon nitride membrane. We use a TEM with a field-emission gun (JEOL JEM-2100F) for the OAM measurements, and operate it at an acceleration voltage of 200 kV. The nanofabricated DVG is inserted into a selected-area aperture position which is the first image plane of the TEM objective lens. The electron diffraction pattern is recorded at a camera length of 100 cm.

III. RESULTS AND DISCUSSION

Figure 1(b) is a TEM image of the binary-amplitude 2D DVG. The bright regions show holes where the film was completely removed by FIB fabrication. Figure 1(c)
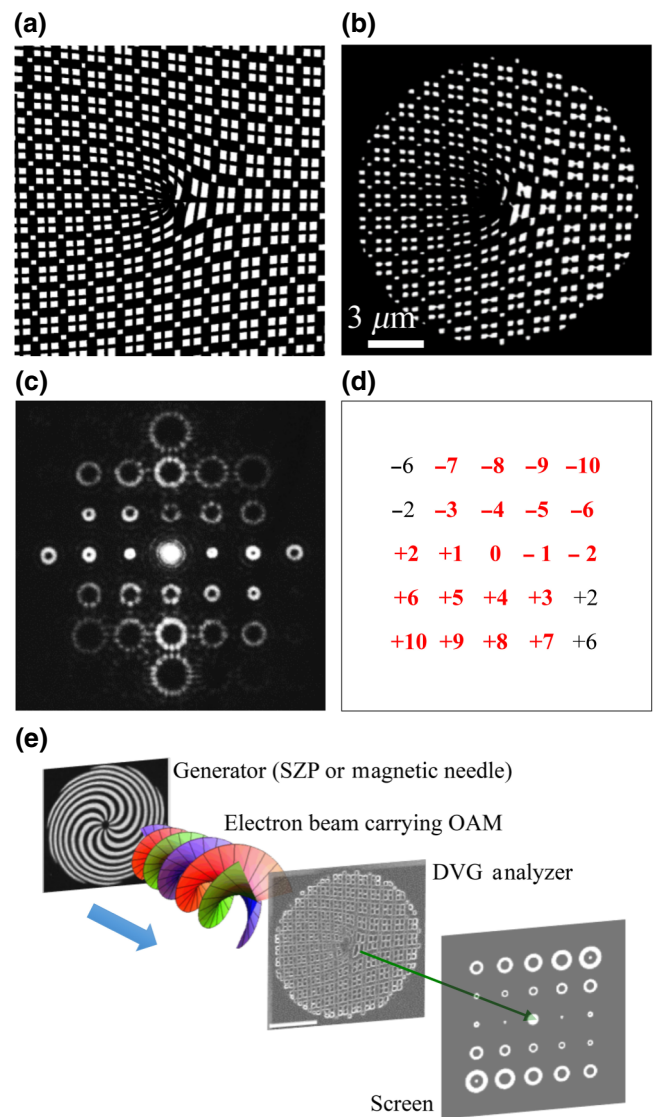

FIG. 1.   (a) Two-dimensional DVG pattern designed by superposing the two 1D DVGs with $m = 1$ and $m = 4$. The DVG pattern was slightly modified by expanding the black region for FIB fabrication. (b) A TEM image of a binary-amplitude 2D DVG with a diameter of about 15 μm, fabricated using a FIB instrument. (c) Experimental electron diffraction pattern from the DVG shown in (b) under a plane wave illumination. (d) The number at the location corresponding to each diffracted beam of the DVG in (c) denotes the OAM value detected for an input beam. The bold numbers in red denote spots used in the spectrum analysis. (e) Schematic illustration of the experiment for measuring electron OAM content via a DVG.

shows a diffraction pattern when the DVG was illuminated by a plane wave. The diffraction pattern reveals an equal-intensity array within the second order of diffraction, except for the transmitted beam. The diffracted beams have ring-shaped intensities, and their radii increase in direct proportion to the absolute values of OAM. In Fig. 1(d), the number at the location corresponding to each diffracted

beam of the DVG shown in Fig. 1(c) denotes the OAM value detected for the input beam. This result indicates that the DVG correctly produces beams with the desired OAM values between $-10\hbar$ and $10\hbar$. Phase analysis of the diffracted beams using a diffractive imaging method [32–34] is consistent with the present result [31].

In order to evaluate the performance of the DVG OAM analyzer, we inject electron beams carrying OAM generated by SZPs into the DVG. The experimental setup for measuring the OAM content of electron beams is shown in Fig. 1(e). The electron diffraction patterns are captured on the charge-coupled device (CCD) camera of the TEM after the electrons pass through the DVG. As mentioned previously, the OAM content of the electron beam can be analyzed by measuring the intensity at each beam center of the diffracted beams passing through the DVG. Our simulation results indicate that lateral misalignment of the incident beam [35–38] should be less than one-eighth of the diameter of the Dammann grating to achieve OAM measurement with an error less than $1\hbar$ (see Ref. [31]). The coherence of the incident beam also affects the accuracy of OAM measurement. Our simulation study shows that the coherence length at the grating plane should be more than 50% of the diameter of the grating to achieve the OAM accuracy of $1\hbar$ (see Refs. [31,39]).

We use a FIB instrument to fabricate SZPs with various topological charges as described previously [14]. Figures 2(a) and 2(b) display scanning ion microscope (SIM) images of the SZPs with topological charges of 6 and 10, respectively. The SZPs are inserted into the condenser aperture position of the TEM. The SZP produces a series of electron beams carrying different OAMs, which are aligned in the direction of the beam propagation [14]. Because the focal depth from the SZP located at the condenser aperture is large, electron beams carrying OAMs of 0, $\pm6\hbar$, ... (0, $\pm10\hbar$, ...) from the SZP with a topological charge of 6 (10) are incident onto the DVG altogether. Here, the illumination condition is set by adjusting the convergence angles of the input electron beam, changing the excitation and alignment of the lens system. Figures 2(c) and 2(d) show the electron diffraction patterns where the electron beams from the SZPs with topological charges of 6 and 10, respectively, are incident onto the DVG [31,40]. The diffraction beams are denoted with (h, k), where h and k are integers. In Fig. 2(c), sharp bright center spots representing beams with zero OAM can be clearly observed, as indicated by the arrows at $(h, k) = (-2, -1)$, $(-2, 2)$, $(2, -2)$, and $(2, 1)$, indicating an OAM of $\pm6\hbar$. In Fig. 2(d), these spots appear at $(h, k) = (-2, -2)$ and $(2, 2)$, indicating an OAM of $\pm10\hbar$. The OAM components can be deduced from the integrated intensity of the regions of interest at each beam center. Figures 2(e) and 2(f) depict the normalized intensity of each center spot as a function of OAM values (OAM spectra). Each of the integrated intensities is obtained from a circular region with
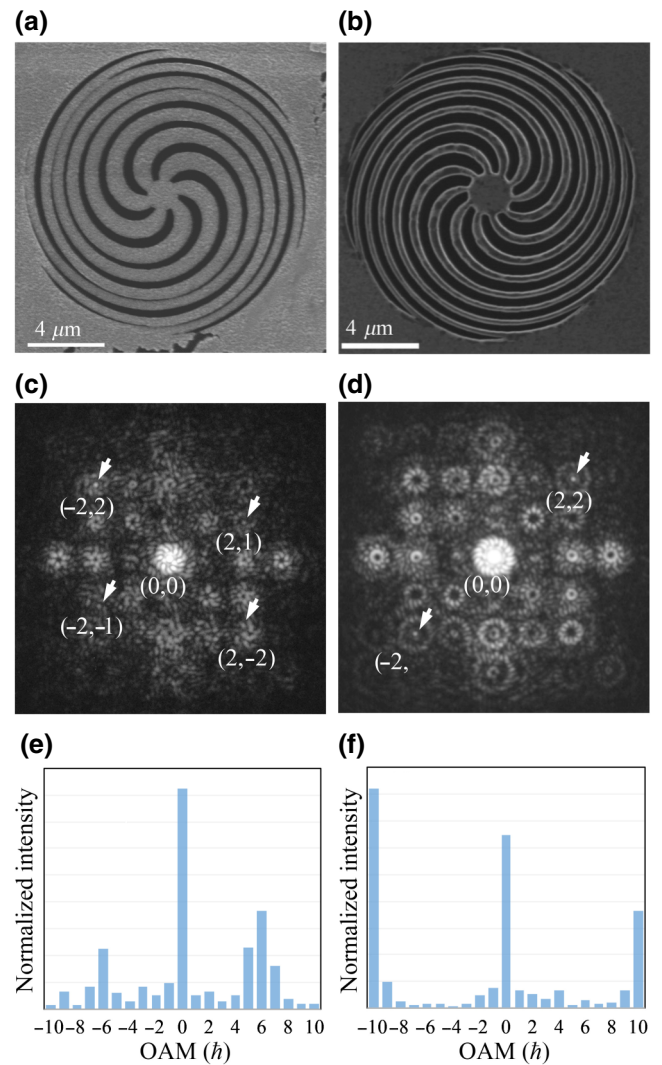

FIG. 2. SIM images of the SZPs fabricated by FIB with a topological charge of (a) 6 and (b) 10, respectively. Electron diffraction patterns when the electron beams through the SZPs with topological charges of 6 (c) and 10 (d) were incident onto the DVG (magnified images and intensity profiles are shown in Supplemental Material [31]). The arrows indicate the detected OAM components. OAM spectrums (e),(f) are obtained from the electron diffraction patterns (c) and (d), respectively, produced with the SZPs.

a radius of $1/4d_{DVG}$, where d_{DVG} indicates the diameter of the DVG. Our simulation studies indicate that the integrated radius should be smaller than half the beam waist of the nonvortex beam diffracted from the DVG, which is $1/d_{DVG}$, to obtain a sharp OAM spectrum [31,41]. The sharpness of the OAM spectrum does not change significantly when the number of electrons used to record the diffraction patterns is more than 10^4. Normalized spectra are prepared by dividing the integrated individual intensity by a reference intensity when the incident beam is a plane wave, after subtracting background noise. As expected,

the electron beams carry OAMs of 0 and $\pm 6\hbar$, as shown in Fig. 2(e), and of 0 and $\pm 10\hbar$, as shown in Fig. 2(f). The ratio of OAM components $\pm 6\hbar$ ($\pm 10\hbar$) is changed by the illumination condition, here especially focusing of the beam into the DVG and the position of the DVG [31]. These experimental results verify that the DVG-OAM analyzer proposed in this study successfully separates an input electron beam, even one composed of multiple OAM components, into its OAM components. We also verify that the DVG works correctly by numerical simulation [31].

One of the significant applications of electrons carrying OAM is to employ them as nanoscale probes in magnetic materials. Conventional methods of probing magnetic materials via electron beams are Lorentz microscopy, electron holography, and the transport of intensity phase imaging [42,43]. Recently, Grillo *et al.* used an electron beam carrying an OAM of $\pm 200\hbar$ to measure a nanoscale out-of-plane magnetic pillar [10]. The magnetic fields of a magnetic bar were examined using a device based on nanoscale holograms for measuring electron OAM components [11]. Here, we use a DVG OAM analyzer to measure the OAM states of electrons affected by a nanofabricated magnetic needle. It has been previously demonstrated that magnetic needles can be used to generate electron beams carrying OAM [15,16]. Magnetic monopoles act as OAM ladder operators, either increasing or decreasing the initial electron OAM state by $\nu = e\Phi/(2\pi\hbar)$, where ν is the integer topological charge of the monopole and Φ is the magnetic flux passing through the area enclosed by the path [10,11]. Figure 3(a) shows an SIM image of the magnetic needle fabricated by using an FIB instrument. The magnetic needle is extracted and fabricated from bulk nickel (Ni) with a thickness of 1 μm by FIB and mounted onto a molybdenum (Mo) circular aperture. The strong shape anisotropy of the magnetic needle leads to a situation where only a single on-axis magnetic domain occurs [16]. The nanofabricated magnetic needle is inserted at the condenser aperture of the TEM. We investigate the electron beams after passing them through a magnetic needle illuminated by a plane wave. First, conventional off-axis electron holography measurements are carried out in order to obtain the phase distribution by the magnetic field around the magnetic needle. A hologram is recorded using a 200 kV TEM (Hitachi HF-2000) equipped with an electron biprism and a cold field-emission gun. Figure 3(b) shows a reconstructed phase distribution around the tip of the magnetic needle. It can be observed that the phase change is spiraling around the tip of the magnetic needle and reaches $6 \times 2\pi$ rad. This phase change must be mainly due to monopolelike magnetic fields.

Next, a beam passing through the magnetic needle is introduced to the DVG, as shown in Fig. 1(e). The beam center is adjusted to be at the center of the DVG. Figure 3(c) shows an electron diffraction pattern of the DVG after passing through the magnetic needle. The
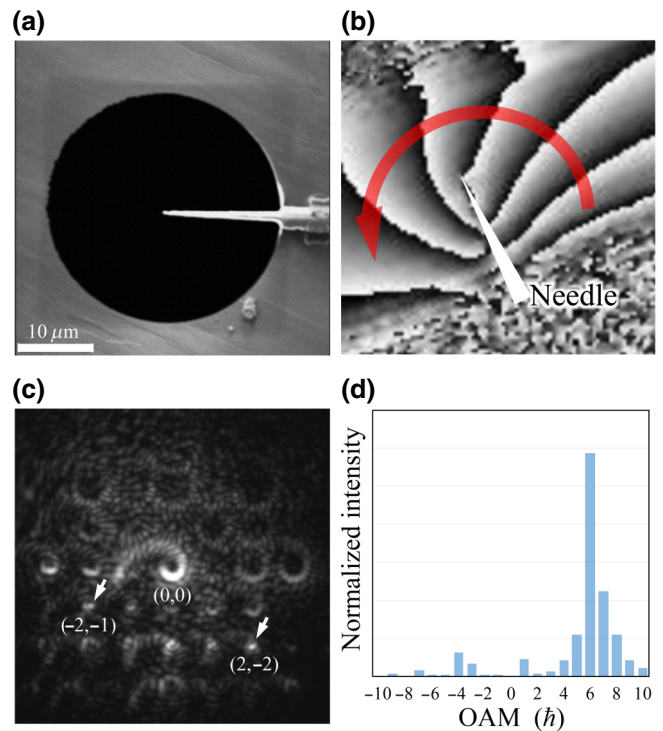

FIG. 3. (a) SIM image of a Ni magnetic needle positioned onto a Mo circular aperture, forming a monopolelike magnetic field. The needle length is about 15 μm, and the tip diameter is about 500 nm. (b) The reconstructed phase distribution around the tip of the magnetic needle by electron holography, obtained in a magnetic field-free condition. White and black regions correspond to phases of 2π and 0, respectively. The phase change due to the magnetic field is spiraling around the tip of the needle and reaches $6 \times 2\pi$ rad. (c) The electron diffraction pattern when the electron beams passing through the magnetic needle are incident onto the DVG. The arrows indicate sharp center spots involving OAM components. (d) The OAM spectrum extracted from the electron diffraction pattern.

diffraction pattern shows sharp spots at $(h, k) = (-2, -1)$ and $(2, -2)$, indicating an OAM of $6\hbar$. The transmitted beam at $(h, k) = (0, 0)$ is not closed, unlike a ring shape, which is expected in ordinary vortex beams. This may be due to the electric charging effect. Figure 3(d) depicts the normalized intensity as a function of OAM. The presented OAM spectrum displays a peak around an OAM of $6\hbar$. The intensity-weighted mean and standard deviation of the peak are evaluated as $6.1\hbar$ and $0.6\hbar$, respectively. Such a sharp spectrum suggests an ideal needle shape. The only positive value of OAM is due to the monopolelike magnetic field induced by the magnetic needle. This result is consistent with that of the phase measurement we obtained through electron holography [31,44]. We note that the shape and thickness of magnetic needles affect the OAM distributions in OAM spectrums. The phase distribution by electron holography can yield a sample's magnetic information and an OAM spectrum. On the other hand, the

proposed OAM detection method allows more direct and informative measurements of a sample's magnetic information. The use of a nonvortex beam with a subnanometer spot size as an incident beam, in conjunction with scanning electron probes, provides an alternative TEM technique to characterize the magnetic properties at the atomic scale.

IV. CONCLUSION

We successfully design and nanofabricate a binary-amplitude 2D DVG for measuring electron OAM states. The proposed DVG-OAM analyzer proves its effectiveness by providing the electron OAM spectrums from the nanofabricated SZPs and magnetic needles. The improvement yielded by the presented method and device could enable the mapping of magnetic distributions of materials at the atomic scale. Furthermore, the proposed configuration could be used for the OAM detection of arbitrary electrons if sufficiently coherent, for instance, in such an atom and a graphene, to measure the OAM of photoelectrons in photoelectron spectroscopy.

ACKNOWLEDGMENTS

[1] M. Uchida and A. Tonomura, Generation of electron beams carrying orbital angular momentum, Nature **464**, 737 (2010).

[2] J. Verbeeck, H. Tian, and P. Schattschneider, Production and application of electron vortex beams, Nature **467**, 301 (2010).

[3] B. J. McMorran, A. Agrawal, I. M. Anderson, A. A. Herzing, H. J. Lezec, J. J. McClelland, and J. Unguris, Electron vortex beams with high quanta of orbital angular momentum, Science **331**, 192 (2011).

[4] Y. Hasegawa, K. Saitoh, N. Tanaka, S. Tanimura, and M. Uchida, Young's interference experiment with electron beams carrying orbital angular momentum, J. Phys. Soc. Jpn. **82**, 033002 (2013).

[5] Y. Hasegawa, K. Saitoh, N. Tanaka, and M. Uchida, Propagation dynamics of electron vortex pairs, J. Phys. Soc. Jpn. **82**, 073402 (2013).

[6] J. Harris, V. Grillo, E. Mafakheri, G. C. Gazzadi, S. Frabboni, R. W. Boyd, and E. Karimi, Structured quantum waves, Nat. Phys. **11**, 629 (2015).

[7] K. Y. Bliokh, I. P. Ivanov, G. Guzzinati, L. Clark, Ruben Van Boxem, Armand Béché, Roeland Juchtmans, M. A. Alonso, P. Schattschneider, F. Nori, and J. Verbeeck, Theory and applications of free-electron vortex states, Phys. Rep. **690**, 1 (2017).

[8] S. M. Lloyd, M. Babiker, G. Thirunavukkarasu, and J. Yuan, Electron vortices: Beams with orbital angular momentum, Rev. Mod. Phys. **89**, 035004 (2017).

[9] B. J. McMorran, A. Agrawal, P. A. Ercius, V. Grillo, A. A. Herzing, T. R. Harvey, M. Linck, and J. S. Pierce, Origins and demonstrations of electrons with orbital angular momentum, Philos. Trans. R. Soc., A **375**, 20150434 (2017).

[10] V. Grillo, T. R. Harvey, F. Venturi, J. S. Pierce, R. Balboni, F. Bouchard, G. Carlo Gaz-zadi, S. Frabboni, A. H. Tavabi, Z.-A. Li, R. E. Dunin-Borkowski, R. W. Boyd, B. J. McMorran, and E. Karimi, Observation of nanoscale magnetic fields using twisted electron beams, Nat. Commun. **8**, 689 (2017).

[11] V. Grillo, A. H. Tavabi, F. Venturi, H. Larocque, R. Balboni, G. C. Gazzadi, S. Frabboni, P.-H. Lu, E. Mafakheri, F. Bouchard, R. E. Dunin-Borkowski, R. W. Boyd, M. P. J. Lavery, M. J. Padgett, and E. Karimi, Measuring the orbital angular momentum spectrum of an electron beam, Nat. Commun. **8**, 15536 (2017).

[12] V. Grillo, G. C. Gazzadi, E. Karimi, E. Mafakheri, R. W. Boyd, and S. Frabboni, Highly efficient electron vortex beams generated by nanofabricated phase holograms, Appl. Phys. Lett. **104**, 043109 (2014).

[13] J. Verbeeck, H. Tian, and A. Béché, A new way of producing electron vortex probes for STEM, Ultramicroscopy **113**, 83 (2012).

[14] K. Saitoh, Y. Hasegawa, N. Tanaka, and M. Uchida, Production of electron vortex beams carrying large orbital angular momentum using spiral zone plates, J. Electron Microsc. **61**, 171 (2012).

[15] A. M. Blackburn and J. C. Loudon, Vortex beam production and contrast enhancement from a magnetic spiral phase plate, Ultramicroscopy **136**, 127 (2014).

[16] A. Béché, R. V. Boxem, G. V. Tendeloo, and J. Verbeeck, Magnetic monopole field exposed by electrons, Nat. Phys. **10**, 26 (2014).

[17] H. Nambu, Y. Noguchi, K. Saitoh, and M. Uchida, Nearly nondiffracting electron lattice beams generated by polygonal slits, Microscopy **66**, 295 (2017).

[18] A. Blackburn, Observation of an electron vortex beam created from a self-charging rod, Microsc. Microanal. **22** (Suppl. 3), 1710 (2016).

[19] G. Pozzi, P. H. Lu, A. Tavabi, M. Duchamp, and R. E. Dunin-Borkowski, Generation of electron vortex beams using line charges via the electrostatic Aharonov-Bohm effect, Ultramicroscopy **181**, 191 (2017).

[20] K. Saitoh, Y. Hasegawa, K. Hirakawa, N. Tanaka, and M. Uchida, Measuring the orbital angular momentum of electron vortex beams using a forked grating, Phys. Rev. Lett. **111**, 074801 (2013).

[21] G. Guzzinati, L. Clark, A. Béché, and J. Verbeeck, Measuring the orbital angular momentum of electron beams, Phys. Rev. A **89**, 025803 (2014).

[22] L. Clark, A. Béché, G. Guzzinati, and J. Verbeeck, Quantitative measurement of orbital angular momentum in electron microscopy, Phys. Rev. A **89**, 053818 (2014).

[23] B. J. McMorran, T. R. Harvey, and M. P. Lavery, Efficient sorting of free electron orbital angular momentum, New J. Phys. **19**, 023053 (2017).

[24] H. Larocque, F. Bouchard, V. Grillo, A. Sit, S. Frabboni, R. E. Dunin-Borkowski, M. J. Padgett, R. W. Boyd, and E. Karimi, Nondestructive measurement of orbital angular momentum for an electron beam, Phys. Rev. Lett. **117,** 154801 (2016).

[25] T. R. Harvey, V. Grillo, and B. J. McMorran, Stern-Gerlach-like approach to electron orbital angular momentum measurement, Phys. Rev. A **95,** 021801(R) (2017).

[26] H. Dammann and E. Klotz, Coherent optical generation and inspection of two-dimensional periodic structures, Opt. Commun. **24,** 505 (1977).

[27] H. Dammann and K. Görtler, High-efficiency in-line multiple imaging by means of multiple phase holograms, Opt. Acta **3,** 312 (1971).

[28] C. Zhou and L. Liu, Numerical study of Dammann array illuminators, Appl. Opt. **34,** 5961 (1995).

[29] N. Zhang, X. C. Yuan, and R. E. Burge, Extending the detection range of optical vortices by Dammann vortex gratings, Opt. Lett. **35,** 3496 (2010).

[30] P. Chen, S. J. Ge, L. L. Ma, W. Hu, V. Chigrinov, and Y. Q. Lu, Generation of equal-energy orbital angular momentum beams via photopatterned liquid crystals, Phys. Rev. Appl. **5,** 044009 (2016).

[31] See Supplemental Material at http://link.aps.org/supplemental/10.1103/PhysRevApplied.12.064062 for (I) the design of the DVG, (II) the phase distribution analysis of the diffracted beams using a diffractive imaging method, (III) the simulations of DVG electron diffraction patterns, (IV) the misalignment evaluation, (V) the beam and integration sizes, beam coherence, noise susceptibility, and radial LG beam, (VI) the integration size by a numerical simulation, (VII) the intensity profiles, and (VIII) the phase distribution and its OAM spectrum.

[32] J. M. Zuo, I. Vartanyants, M. Gao, R. Zhang, and L. A. Nagahara, Atomic resolution imaging of a carbon nanotube from diffraction intensities, Science **300,** 1419 (2003).

[33] J. Yamasaki, K. Ohta, S. Morishita, and N. Tanaka, Quantitative phase imaging of electron waves using selected-area diffraction, Appl. Phys. Lett. **101,** 234105 (2012).

[34] R. W. Gerchberg and W. O. Saxton, Phase determination for image and diffraction plane pictures in the electron microscope, Optik **34,** 275 (1971).

[35] M. V. Vasnetsov, V. A. Pas'ko, and M. S. Soskin, Analysis of orbital angular momentum of a misaligned optical beam, New J. Phys. **7,** 46 (2005).

[36] J. Lin, X.-C. Yuan, M. Chen, and J. C. Dainty, Application of orbital angular momentum to simultaneous determination of tilt and lateral displacement of a misaligned laser beam, J. Opt. Soc. Am. A **27,** 2337 (2010).

[37] G. Anzolin, F. Tamburini, A. Bianchini, and C. Barbieri, Method to measure off-axis displacements based on the analysis of the intensity distribution of a vortex beam, Phys. Rev. A **79,** 033845 (2009).

[38] P. Zhao, S. Li, Y. Wang, X. Feng, C. Kaiyu, W. Zhang, and Y. Huang, Identifying the tilt angle and correcting the orbital angular momentum spectrum dispersion of misaligned light beam, Sci. Rep. **7,** 7873 (2017).

[39] T. Latychevskaia, Spatial coherence of electron beams from field emitters and its effect on the resolution of imaged objects, Ultramicroscopy **175,** 121 (2017).

[40] M. Born and E. Wolf, *Principles of Optics* (Pergamon, New York, 1970).

[41] S. Topuzoski and L. Janicijevic, Fraunhofer diffraction of a Laguerre–Gaussian laser beam by fork-shaped grating, J. Mod. Opt. **58,** 138 (2011).

[42] M. Uchida, Y. Onose, Y. Matsui, and Y. Tokura, Real-space observation of helical spin order, Science **311,** 359 (2006).

[43] M. Beleggia, T. Kasama, and R. E. Durin-Borkowski, The quantitative measurement of magnetic moments from phase images of nanoparticles and nanostructures—I. Fundamentals, Ultramicroscopy **110,** 425 (2010).

[44] E. Yao, S. Franke-Arnold, J. Courtial, S. Barnett, and M. Padgett, Fourier relationship between angular position and optical orbital angular momentum, Opt. Express **14,** 9071 (2006).